Journal of Industrial and Engineering Chemistry 65 (2018) 195–204

Contents lists available at ScienceDirect

Journal of Industrial and Engineering Chemistry

journal homepage: www.elsevier.com/locate/jiec

Significant impact of monomer curvatures for polymer curved shape composition on backbone orientation and solar cell performances

Tae Ho Lee, Doo Hun Kim, Eui Jin Lee, Doo Kyung Moon*

Department of Material Chemistry and Engineering, Konkuk University, Seoul, 143-701, Republic of Korea

ARTICLE INFO

Article history:
Received 7 November 2017
Received in revised form 3 April 2018
Accepted 18 April 2018
Available online 28 April 2018

Keywords:
Organic photovoltaics (OPVs)
Quinacridone (Qc)
Benzo [2,1-b:3,4-b'] dithiophene (BDP)
π spacer
Density functional theory (DFT)
Shape curvature

ABSTRACT

In the present study, linear or curve-shaped donor units, quinacridone (Qc) and benzo[2,1-b:3,4-b′] dithiophene (BDP), and spacers were introduced for polymerization of four D–A type polymers (PBDPOx-biT, PBDPOx-TT, PQcOx-biT, and PQcOx-TT).

The UV–vis absorption spectra of PBDPOx-biT, PQcOx-TT (linear shaped polymer) films were red-shifted compared with the solution absorption, whereas that of a PBDPOx-TT, PQcOx-biT (curve shaped polymer) film was blue-shifted. PBDPOx-biT, PQcOx-TT had high crystallinity. Linear polymers prefer regular and crystalline domains in the film state and lead to more efficient organic photovoltaic (OPV) devices. PQcOx-TT possesses a PCE value of up to 3.4%.

Introduction

Organic semiconductor materials have attracted considerable attention over the past several decades for their advantages of ease of structural transformation since the discovery of π-conjugated electrical conductivity, good light absorption and emission characteristics, reduced production cost through solution process, being lightweight, and allowing fabrication of devices with flexibility. They have been used in the optoelectronic field as light emitting diodes (LEDs) [1,2], field effect transistors (TFTs) [3,4], solar cells [5], and optical sensors [6]. Among them, various studies have been conducted on low-bandgap (LBG) donor polymer using push–pull effect and organic photovoltaics (OPVs) [7–10] with structure from bulk heterojunction (BHJ) of fullerene derivative such as tuning the alternating conjugated donor–acceptor (D–A) main chain derivatives and side chains for changes in absorption region according to changes in bandgap, high carrier mobility, and energy level control, as well as achieving high efficiency by increasing J_{SC}, Voc, and FF through controlling the alignment of material in devices [11–14]. Using donor polymers that use various derivatives, such as benzothiadiazole (BT), benzooxadiazole (Ox), diketopyrrolopyrrole (DPP), isoindigo (In), thiazolothiazole (TTZ), and thienopyrroledione (TPD), these studies reported polymers and devices with 4–11% PCE [15–17].

For reproduction of OPVs with high efficiency, PCE was improved by improving Voc and J_{SC} through studies that adequately match the energy level and 6,6-phenyl C-butyric acid methyl ester (PCBM), used mostly as acceptor material, along with achieving LBG for wide absorption range from material perspective.

However, recent studies have reported on increasing J_{SC} values by reducing exiton recombination and improving the mobility of electrons in the direction of electrodes by forming a face-on structure through changes in π-stacking characteristics in film and material solubility, while changing the side chains and side functional units of material [18,19].

According to a study by Wang et al., it was confirmed that the geometry of polymer main chain changed according to thiophene and thieno[3,2-b]thiophen introduced on BDT and BT. Accordingly, changes in optical property and film orientation were also confirmed [20,21]. Moreover, our laboratory also confirmed that geometry changed according to 3 types of π-spacers, resulting in changes in J_{SC} and PCE [22,23].

The present study aimed to confirm not only changes in geometry by π-spacer, but also changes in polymer curvature according to the type of D–A monomer. Based on studies that showed improved J_{SC} from π-spacer relieving steric hindrance, it was confirmed that the curvature of polymer main chain can be controlled by selecting the π-spacer that match the curvature of D–A monomer. Accordingly, the present study examined measures that can improve J_{SC} in the polymer design process. Liner donor quinacridone and curved donor BDP were introduced to Ox, a

* Corresponding author.
E-mail address: dkmoon@konkuk.ac.kr (D.K. Moon).

https://doi.org/10.1016/j.jiec.2018.04.029
1226-086X/

typical strong electron accepting monomer with linear structure. Moreover, liner thieno[3,2-b]thiophen (TT) π-spacer and curved 2,2′-bithiophen (biT) π-spacer were introduced on polymer to prevent intramolecular steric hindrance, and studied the method for optimizing the curvature according to the type of donor and π-spacer within the polymer. To identify the changes in polymer curvature according to the type of donor and π-spacer, 4 polymers, poly(4,5-Di(2-ethylhexyloxy)benzo[2,1-b:3,4-b′]dithiophene-5,6-bis(octyloxy)-4,7-di(thieno[3,2-b]thiophen-2-yl)benzo[c][1,2,5] oxadiazole (PBDPOx-TT), poly(4,5-Di(2-ethylhexyloxy)benzo[2,1-b:3,4-b']dithiophene-4,7-di(2,2'-bithiophen-5-yl)-5,6-bis(octyloxy)benzo[c][1,2,5]oxadiazole (PBDPOx-biT), poly(5,12-bis(2-octyldodecyl)quinolino[2,3-b]acridine-7,14-dione-5,6-bis(octyloxy)-4,7-di(thieno[3,2-b]thiophen-2-yl)benzo[c][1,2,5]oxadiazole) (PQcOx-TT) and poly(5,12-bis(2-octyldodecyl)quinolino[2,3-b]acridine-7,14-dione-4,7-di(2,2'-bithiophen-5-yl)-5,6-bis(octyloxy)benzo[c][1,2,5]oxadiazole) (PQcOx-biT) were polymerized. Moreover, polymerized polymers were used to fabricate OPVs devices and their characteristics were evaluated. It was found that J_{SC} and FF showed differences according to the type of donor and π-spacer and consequent changes in curvature of the entire polymer. From this, it was confirmed that charge transport characteristics changed according to changes in polymer alignment.

Experimental section

Measurements

Unless otherwise specified, all reactions were performed under a nitrogen atmosphere. The solvents were dried using the standard procedures. All column chromatography was performed with silica gel (230–400 mesh, Merck) as the stationary phase. ^{1}H NMR (400 MHz) spectra were recorded with a Bruker AMX400 spectrometer, using the resonances of the solvent as an internal reference. Chemical shifts (d) are reported in ppm downfield from TMS. The molecular weights of the polymers were measured using the GPC method with polystyrene standards. TGA measurements were performed on a TA Instruments 2050 analyzer. Electrochemical cyclic voltammetry was performed using a Zahner IM 6e electrochemical workstation with 0.1 M Bu_4NPF_6 in acetonitrile as the electrolyte. ITO glass coated with a thin polymer film was used as the working electrode, and a Pt wire and an Ag/Ag^+ electrode were used as the counter and reference electrodes, respectively. The electrochemical potential was calibrated against Fc/Fc^+. Current–voltage (I–V) curves of the PSC devices were measured using a computer-controlled Keithley 2400 source measurement unit equipped with a Peccell solar simulator under AM1.5G illumination (100 mW/cm^2). The illumination intensity was calibrated using a standard Si photodiode detector equipped with a KG-5 filter. The output photocurrent was adjusted to match the photocurrent of the Si reference cell to obtain a power density of 100 mW/cm^2. After encapsulation, all devices were operated under ambient atmospheric conditions at 25 °C.

Fabrication and treatment of polymer solar cells

All of the BHJ PV cells were prepared using the following device fabrication procedure. The glass/indium tin oxide (ITO) substrates [Sanyo, Japan (10 X/c)] were lithographically patterned, cleaned with detergent, and sonicated in deionized water, acetone, and isopropyl alcohol. The substrates were then dried on a hot plate at 120 °C for 10 min and treated with oxygen plasma for 30 min to improve the contact angle immediately before the film coating process. Poly(3,4-ethylene-dioxythiophene): poly(styrene-sulfonate) (PEDOT:PSS, Baytron P 4083 Bayer AG) was passed through a 0.45-lm filter before being deposited onto the ITO substrates at a thickness of ca. 32 nm by spin-coating at 4000 rpm in air and then dried at 120 °C for 20 min inside a glove box. The solutions were then passed through a 0.45-lm PTFE filter and spin-coated (500–4000 rpm, 30 s) on top of the PEDOT:PSS layer device fabrication was completed by depositing layers of Al (200 nm) at pressures of less than 10^{-6} torr. The active area of the devices was 4.0 mm^2. Finally, the cell was encapsulated using a UV-curing glue (Nagase, Japan). The conventional devices were fabricated with the following structure: ITO glass/PEDOT:PSS/polymer:$PC_{70}BM$(active layer)/BaF_2/Ba/Al encapsulation glass. The inverted devices were fabricated with the following structure: ITO glass/ZnO/polymer: $PC_{70}BM$(active layer)/MoO_3/Al encapsulation glass.

Synthesis and characterization of polymers

Scheme 1 shows the chemical structures of monomers and polymers, along with synthetic routes. As the donor, 2,7-bis (trimethyltin)-4,5-di(2-ethylhexyloxy) benzo[2,1-b:3,4-b']dithiophene (BDP, D1), 5,12-bis(2-octyldodecyl)-2,9-bis(4,4,5,5-tetramethyl-1,3,2-dioxaborolan-2-yl)quinolino[2,3-b]acridine-7,14(5H, 12H)-dione (Qc, D2) was synthesized. As the acceptor, thieno[3,2-b]thiophene and thiophene π spacer were introduced to 4,7-dibromo-5,6-bis(octyloxy)benzo[c][1,2,5]oxadiazole to synthesize 4,7-bis(5-bromothieno[3,2-b]thiophen-2-yl)-5,6-bis(octyloxy) benzo[c][1,2,5]oxadiazole (Qx-TT, A1) and 4,7-bis(5′-bromo-2,2′-bithiophen-5-yl)-5,6-bis(octyloxy)benzo[c][1,2,5]oxadiazole (Qx-biT, A2). The monomer used was synthesized by literature methods [22–29]. For polymerization, Stille coupling was performed for 48 h at 90 °C using $Pd_2(dba)_3$ and P(o-tol)$_3$ as the catalysts and toluene as the solvent, while Suzuki coupling was performed for 48 h at 90 °C using $Pd(PPh_3)_4$ as the catalyst, THF as the solvent, 2 M aqueous K_2CO_3 base, and Aliquat 336 as the surfactant. After polymerization was completed, end-capping was performed for 3 h each with 2-bromothiophene and tributhyl stannyl thiophene. The obtained powders were retrieved by precipitating them again in methanol. Also, Soxhlet apparatus was used for purification of methanol, acetone, and chloroform, in that order. Finally, the polymer powders obtained from retrieving chloroform-soluble portion showed a yield of 72–88%. The polymers dissolved well in general organic solvents, such as THF, chloroform, chlorobenzene, and *o*-dichlorobenze. Synthesized monomer and polymer structures were identified through ^{1}H NMR.

4,5-Di(2-ethylhexyloxy)benzo[2,1-b:3,4-b′]dithiophene (2)

Compound 2 (0.35 g, 1.14 mmol), cesium carbonate (3.7 g, 11.42 mmol), and 2-ethylhexyl bromide (2.0 mL, 11.42 mmol) were dissolved in 20 mL acetonitrile. The reaction mixture was stirred at 75 °C. 2-Ethylhexyl bromide and cesium carbonate were added more and the mixture was refluxed to 75 °C for further 24 h. The mixture was cooled to room temperature and acetonitrile was removed by rotary evaporation. The residue was partitioned between water and dichloromethane. The organic phase was washed with 1 M HCl and then with water, dried over Na_2SO_4. Evaporation of the solvent led to a brown oil. The product was purified by column chromatography (*n*-hexane–MC 1: 1). Pure product 2 (0.41 g, 0.912 mmol, 80%) was obtained as a white solid. ^{1}H NMR (400 MHz, $CDCl_3$): 7.50 (d, 2H), 7.35 (d, 2H), 4.06 (m, 4H), 1.81(m, 2H), 1.67(m, 2H), 1.55(m, 6H), 1.36(m, 8H), 0.95 (m, 13H). m/z 446.

2,7-Bis(trimethyltin)-4,5-di(2-ethylhexyloxy)benzo[2,1-b:3,4-b′] dithiophene (BDP, D1)

Compound 2 (0.45 g, 1.0 mmol) was dissolved in 5 mL dry THF. The slightly yellow solution was cooled to −78 °C and *n*-BuLi (1.0 mL, 2.5 mmol, 2.5 M in hexane) was added over 30 min. The

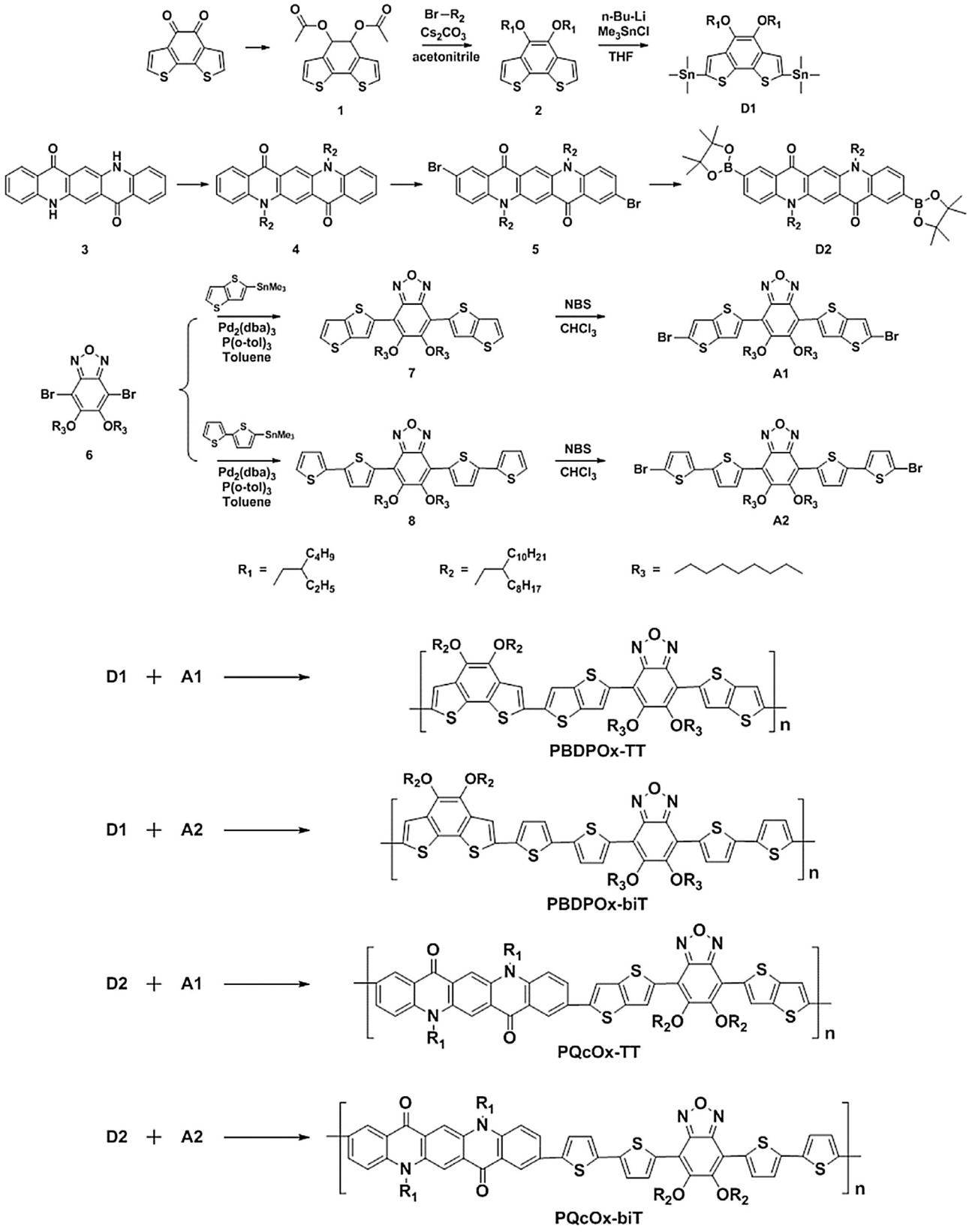

Scheme 1. Synthesis and characterization of monomers and polymers.

suspension was stirred for 1.0 h at −78 °C and 1.0 h at room temperature. After cooling to −78 °C trimethylstannyl chloride 1.0 M in THF (2.5 mL, 2.5 mmol) was added in one portion. The mixture was stirred for 1 h at −78 °C and at room temperature overnight. A ivory solution was formed and *n*-hexane were added for quenching. The suspension was washed with water, dried over Na_2SO_4 and the solvent was removed by evaporator. The product was dried in high vacuum to obtain 780 mg (0.68 mmol, 90%) of a white solid of D1, which was used in the next step without further purification. ^{1}H NMR (400 MHz, $CDCl_3$): 7.54 (s, 2H), 4.06 (d, 4H),

1.52 (t, 4H), 1.43 (s, 2H), 1.37 (m, 10H), 0.97 (t, 8H), 0.94 (m, 8H), 0.44 (t, 24H).

5,6-Bis(octyloxy)-4,7-di(thieno[3,2-b]thiophen-2-yl)benzo[c][1,2,5] oxadiazole (7)

A0 (0.826 g, 1.5 mmol), trimethyl(thieno[3,2-b]thiophen-2-yl) stannane (1.000 g 3.3 mmol) and bis(triphenylphosphine)palladium(II) chloride (0.21 g, 0.3 mmol) were dissolved in 60 mL of anhydrous THF in a well-dried round flask under nitrogen atmosphere. After flushing with nitrogen, the reactant was heated to reflux for 24 h. After cooled to room temperature, the reaction mixture was poured into water. The product was extracted with ethyl acetate. The extracts were combined and washed with water and brine, then dried over Na_2SO_4. The filtrate was concentrated under reduced pressure. The residue was purified by column chromatography on silica to give compound as a deep red oil (0.893 g, 89%). ^{1}H NMR (400 MHz, $CDCl_3$):δ (ppm) 8.80 (s, 2H), 7.46 (d, 2H), 7.31 (d, 2H), 4.16 (t, 4H), 1.98 (m, 4H), 1.455 (m, 4H), 1.33–1.28 (m, 16H), 0.89 (t, 6H).

4,7-Di(2,2′-bithiophen-5-yl)-5,6-bis(octyloxy)benzo[c][1,2,5] oxadiazole (8)

A0 (0.826 g, 1.5 mmol), 2,2′-bithiophen-5-yltrimethylstannane (1.086 g 3.3 mmol) and bis(triphenylphosphine)palladium(II) chloride (0.21 g, 0.3 mmol) were dissolved in 60 mL of anhydrous THF in a well-dried round flask under nitrogen atmosphere. After flushing with nitrogen, the reactant was heated to reflux for 24 h. After cooled to room temperature, the reaction mixture was poured into water. The product was extracted with ethyl acetate. The extracts were combined and washed with water and brine, then dried over Na_2SO_4. The filtrate was concentrated under reduced pressure. The residue was purified by column chromatography on silica to give compound as a deep red crystal (0.995 g, 92%). ^{1}H NMR (400 MHz, $CDCl_3$): δ (ppm) 8.51 (d, 2H), 7.31 (d, 2H), 7.29 (d, 2H), 7.27 (d, 2H), 7.07 (t, 2H), 4.17 (t, 4H), 1.98 (m, 4H), 1.50 (m, 4H), 1.36–1.29 (m, 16H), 0.88 (t, 6H).

4,7-Bis(5-bromothieno[3,2-b]thiophen-2-yl)-5,6-bis(octyloxy)benzo [c][1,2,5] oxadiazole (A1)

Compound 7 (1.338 g, 2 mmol) was added to a mixture of chloroform (100 mL) and acetic acid (100 mL). After *N*-bromosuccimide (0.783 g, 4.4 mmol) was added, the mixture was stirred at room temperature in dark overnight. Then the reaction mixture was poured into water and extracted with chloroform. The extracts were combined and washed with water and saturate sodium bicarbonate solution then dried over Na_2SO_4. After filtration, the solvent in filtrate was removed under reduced pressure. The residue was purified by column chromatography on silica gel to give compound as a dark red oil (1.406 g, 85%). ^{1}H NMR (400 MHz, $CDCl_3$): δ (ppm) 8.75 (s, 2H), 7.33 (s, 2H), 4.15 (t, 4H), 1.96 (m, 4H), 1.45 (m, 4H), 1.33–1.25 (m, 16H), 0.89 (t, 6H).

4,7-Bis(5'-bromo-2,2'-bithiophen-5-yl)-5,6-bis(octyloxy)benzo[c] [1,2,5]oxadiazole (A2)

Compound 5 (1.442 g, 2 mmol) was added to a mixture of chloroform (100 mL) and acetic acid (100 mL). After *N*-bromosuccimide (0.783 g, 4.4 mmol) was added, the mixture was stirred at room temperature in dark overnight. Then the reaction mixture was poured into water and extracted with chloroform. The extracts were combined and washed with water and saturate sodium bicarbonate solution then dried over Na_2SO_4. After filtration, the solvent in filtrate was removed under reduced pressure. The residue was purified by column chromatography on silica gel to give compound as a dark red crystal (1.424 g, 81%). ^{1}H NMR ($CDCl_3$): δ (ppm) 8.50 (d, 2H), 7.23 (d, 2H), 7.03 (m, 4H), 4.16 (t, 4H), 1.96 (m, 4H), 1.49 (m, 4H), 1.33–1.29 (m, 16H), 0.89 (t, 6H).

Results and discussion

Molecular and thermal properties

Table 1 shows the results from measurements on the molecular weights (MWs) of the polymers. The Mn of the polymers was 13,500–32,800 g/mol and PDI was 1.82–2.69. The polymers that used TT spacer showed relatively lower MW and higher PDI. Wang et al. reported that because acceptors with TT are less soluble than acceptors with biT, they showed lower degree of polymerization [16]. However, the difference in solubility according to spacer type was reduced by introducing octyloxy side chain of benzo[c][1,2,5]oxadiazole and minimized the reduction in MW similar to the results that showed similar degree of polymerization [22]. Through this, $\geq$10 polymerization suitable for OPVs device was confirmed. Moreover, the transition temperatures (T_d) of 4 types of polymer under N_2 atmosphere were found to be 300–331 °C (Fig. S1). All of the 4 types of polymers obtained were found to have temperatures suitable for opto-electronic devices fabrication and application.

Electronic structure calculations of the polymers

A simulation was performed using density functional theory (DFT) for examination of the electrical properties of the polymers, molecular geometries, and calculation of electron density of HOMO and LUMO energy level. DFT calculation was performed using hybrid B3LYP correlation functional and Gaussian 09 as the split valence 6-31G(d) basis set. Oligomers with 1 repeating unit were used as the calculation model. The calculated dihedral angle, HOMO and LUMO orbitals are shown in Figs. 1, 2, S2 and Table 2.

As shown in Fig. 1(a), the most stable structure when each derivative was connected was examined by calculating the energy levels according to dihedral angles between the donor unit (Qc or BDP) and spacer and between acceptor unit (Ox) and π-spacer. Moreover, through this, curved formation of monomers using in the present study were shown in Fig. 1(b). Based on this calculation, it was learned that monomer formation was divided into linear and curved shape monomers. Monomers with conjugation direction that was linear were TT, Ox and Qc, while curved monomers were biT and BDP.

As shown in Fig. 2(a), dihedral angles 0.4–26.49° formed in the main chain of the polymers, and conformational locks

Table 1
Physical properties of the polymers.

Polymer	Mn[a] [g/mol]	Mw[a] [g/mol]	PDI[a]	Degree of polymerization	T_d (°C)
PBDPOx-TT	13,500	36,300	2.69	12.3	305
PBDPOx-biT	21,900	42,600	1.95	19.0	331
PQcOx-TT	19,300	51,700	2.68	12.7	302
PQcOx-biT	32,800	59,800	1.82	20.8	300

[a] Determined by GPC in chloroform using polystyrene standards.

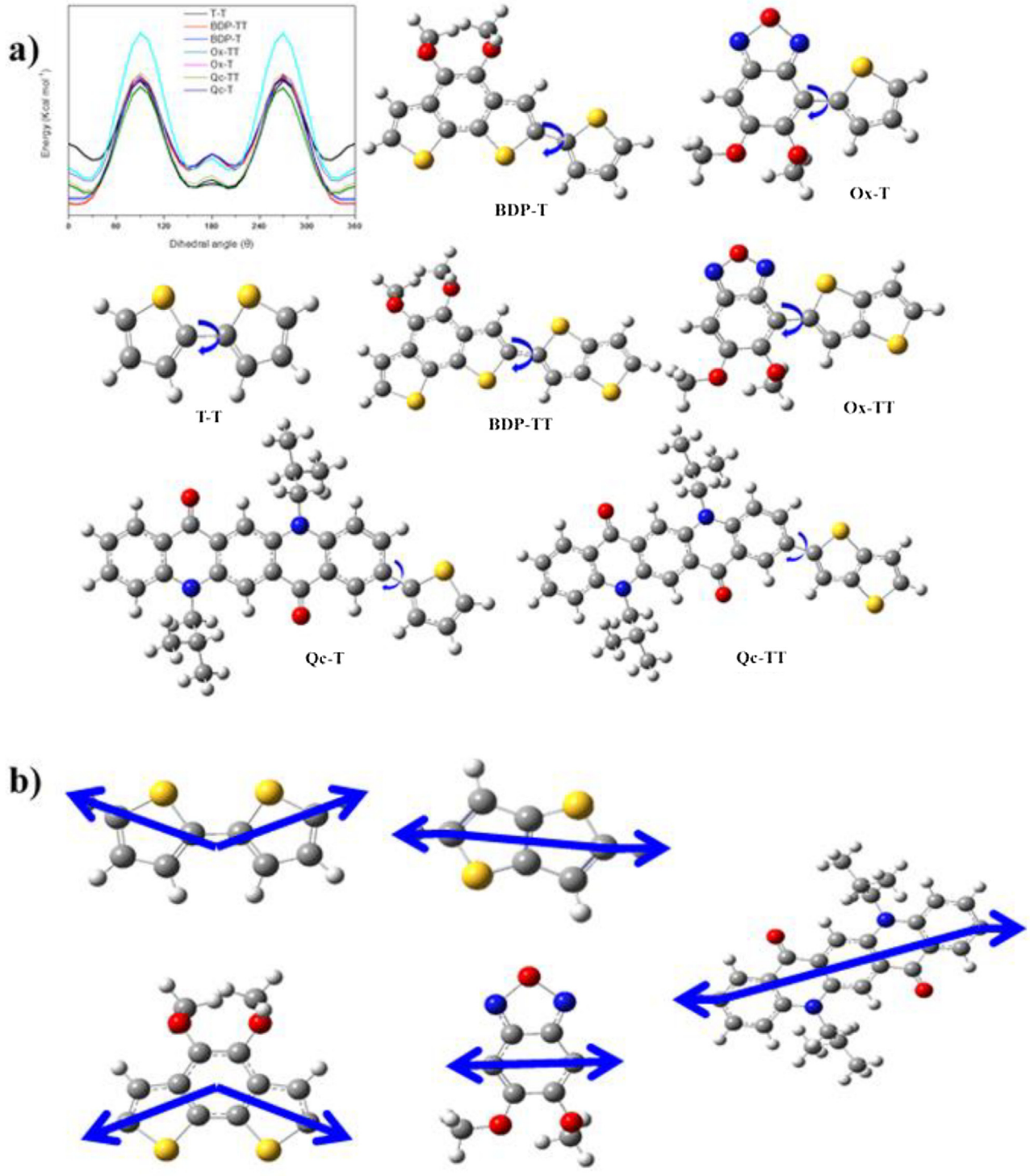

Fig. 1. DFT simulation for tilt angle and conjugation direction of monomers.

Table 2
Calculated parameters.

Polymer	Dihedral angle (deg)					HOMO cal. (eV)	LUMO cal. (eV)
	θ_1	θ_2	θ_3	θ_4	θ_5		
PBDPOx-TT	26.49	6.75	5.22			−5.03	−2.61
PBDPOx-biT	10.24	4.20	9.95	1.59	10.27	−4.97	−2.62
PQcOx-TT	0.40	0.74	0.47			−4.99	−2.78
PQcOx-biT	21.79	18.80	4.22	15.17	4.22	−5.03	−2.67

formed from interactions among S of thiophene, N of BT, S of O/BDP, and O, which resulted in formation of chain with an overall planer shape. This was consistent with the result for a study by Woo et al., in which the curvature of the main backbone became planar due to nonbonding interactions [30–32]. However, the present study found that the dihedral angle of the entire main chain can be altered by not only nonbonding interactions, but by the shapes of the donor, acceptor and π-spacer as well. In Fig. 2(b), the angle between 2 repeating units was 14.5° and 9.4° for PBDPOx-biT and PQcOx-TT (linear shaped polymer),

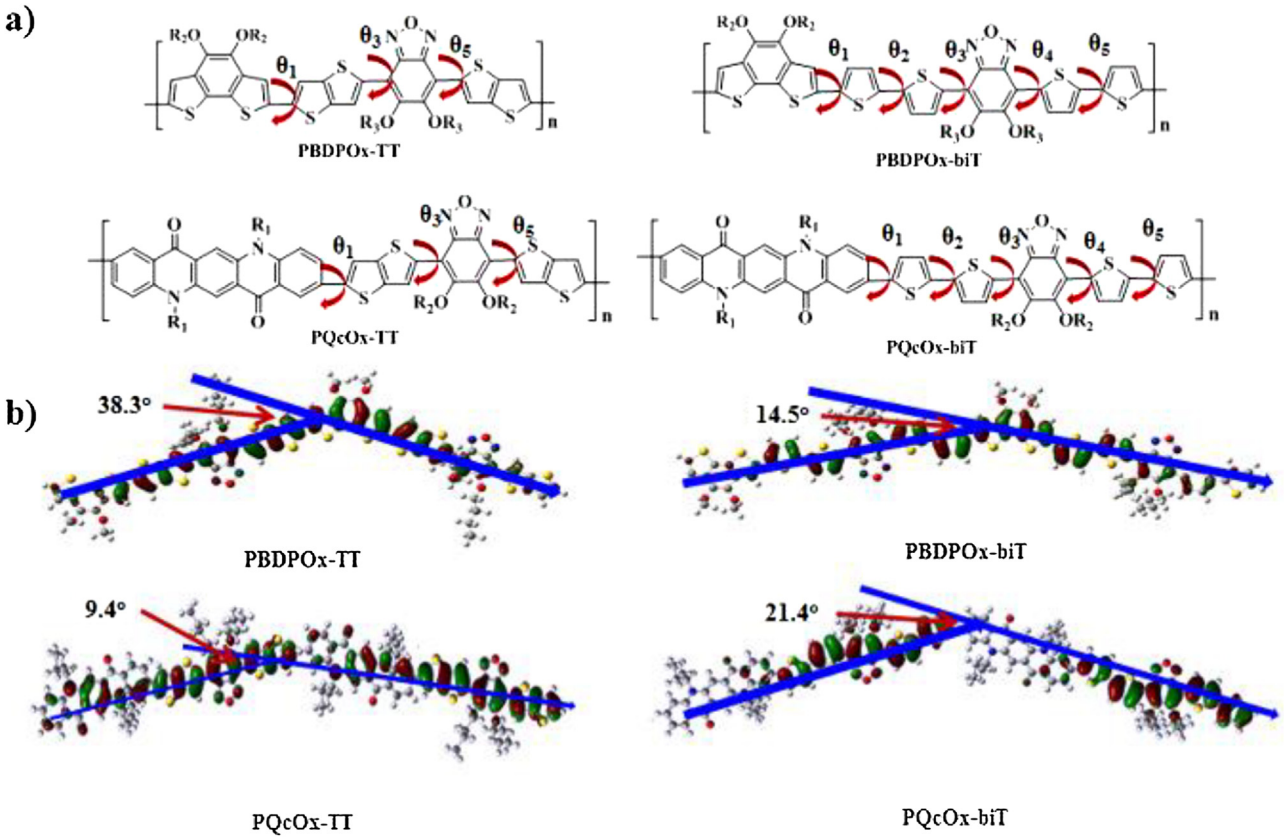

Fig. 2. DFT simulation for tilt angle and electron cloud of polymers.

respectively, showing formation of linear polymer with small curved angle. In contrast, the angle for PBDPOx-TT and PQcOx-biT (curve shaped polymer) was 38.3° and 21.4°, respectively, showing curved polymer structure with relatively large curvature angle. PBDPOx-biT and PQcOx-TT with linear formation showed dihedral angle of 0.40–10.24°, which was smaller than dihedral angle of 4.22–26.49° found in PBDPOx-TT and PQcOx-biT with curved formation. This was expected to reduce the steric hindrance between the polymer main chains and increase the intermolecular interactions between the polymer chains to improve their crystallinity and allow ordered orientation [33,34]. Therefore, it was suspected that PBDPOx-biT and PQcOx-TT used 0 and 2 curved monomers for form a linear polymer structure, while PBDPOx-TT and PQcOx-biT used 1 curved monomer to form a curved polymer structure. In other words, 2n (n = 0,1, . . .) curved monomers must be used to ensure the formation polymers with the main chains that have an overall linear structure. In the present study, improvements in J_{SC} and PCE were expected from orientation in film state according to curved shape of the main backbone.

In Fig. S2, the electrons in HOMO orbitals are delocalized throughout the entire polymer main chain. On the other hand, the electronic cloud in LUMO orbitals are localized on the acceptor monomer side within the polymer. This was due to the accepting effect from the structural characteristics of quinoid formed between N-conjugated electron pair on the Ox unit and electron-withdrawing characteristics of O. This tendency appears throughout entire π-conjugated organic materials with push–pull form [35,36]. Therefore, all of the polymers polymerized in the present study show push–pull form of electron transport within the main chain. The HOMO energy levels of 4 polymers were calculated to be −5.03 to −4.97 eV.

Optical-electrochemical properties

For examination of effects related to the photo physical properties of main chain curved shape according to the combination of BDP, Qc and Ox based polymers, normalized UV–vis spectra of polymers in chloroform solution and on spin-coated thin film were observed. The results are shown in Fig. 3 and summarized in Table 3. For all polymers, UV absorbance in solution state with 4 different water concentrations were measured for calculation of molar absorption coefficient (ε) (Fig. S3). The polymers showed absorption peaks (λ_{max} = 330–450 nm) from localized π–π* transitions and absorption peaks (λ_{max} = 500–700 nm) attributed to intramolecular charge transfer (ICT) transition between D–A units. Since the same Ox accepting unit was used, the ICT absorption peaks showed similar patterns. The π–π* transitions absorption peak appeared strong when Qc unit was used. In solution state, the 4 polymers showed λ_{max} of 550–569 nm, whereas on film, λ_{max} was 547–591 nm. For the film, the maxima absorption spectra of PBDPOx-biT and PQcOx-TT (linear shaped polymer) were red-shifted by 9–22 nm compared with the solution. These results are explained by their much more planar conformations in the solid state. This red shift indicates that PBDPOx-biT and PQcOx-TT (linear shaped polymer) has a strong π-stacking tendency due to aggregation of the polymer in the solid state In contrast, PBDPOx-TT and PQcOx-biT (curve shaped polymer) showed λ_{max} absorption peak being blue-shifted by 1 and 3 nm, respectively. As reported in a previous study by our research group [37] and other studies by Guo et al., Zhang and Matzger and Prlj et al., this was due to steric hindrance

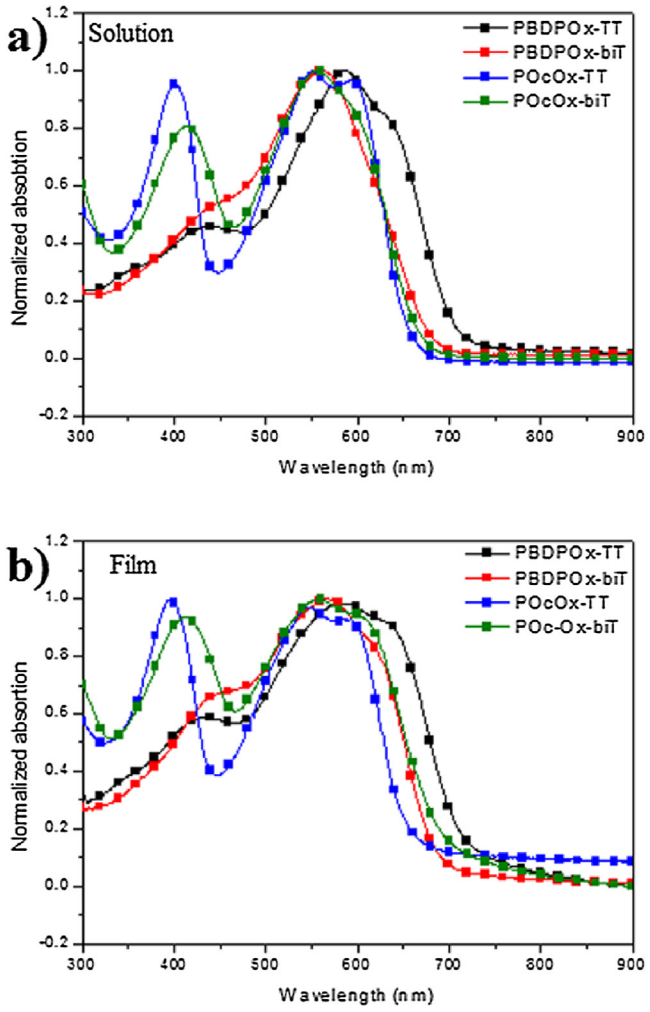

Fig. 3. Normalized UV–vis absorption of the copolymers (a) in chloroform solution and (b) thin film.

interfering with intermolecular overlapping of π-electrons [38–40]. Moreover, this was consistent with intermolecular ordering from liner and curved conformation of the main chains in the DFT calculation. Liner curvature of polymers make intermolecular overlapping of π-electrons relatively easier and tend to show red-shifting, whereas curved curvature of polymers show slight blue-shift since it is difficult to created intermolecular interaction.

The electrochemical properties of the polymers were identified via cyclic voltammogram (CV) spectroscopy. The polymer film formed by drop-casting the polymer dissolved in $CHCl_3$ onto ITO glass electrode was used as the working electrode. This was measured in 0.1 M tetrabutylammonium-hexafluorophosphate (TBAHFP) in acetonitrile solution under N_2 atmosphere. The measured CV results are shown in Fig. S4 and summarized in Table 3. The oxidation onset potential (E^{ox}_{onset}) of PBDPOx-TT, PBDPOx-biT, PQcOx-TT and PqcOx-biT was +0.90, +0.86, +0.99 and +0.84 V, respectively, while the calculation results of their high occupied molecular orbital (HOMO) energy level was −5.30, −5.26, −5.39 and −5.24 eV, respectively. Since the polymers show low HOMO level below −5.24 eV, excellent oxidation stability applicable to OPVs is expected. LUMO was calculated as the diffreence in UV band gaps. The results were consistent with the study by Brocks et al., which reported that intramolecular π conjugation length increased and band gap decreased according to the degree of polymerization, as well as being consistent with results of having band gap that is lower than the DFT result [41]. Furthermore, it was also confirmed that the results were consistent with DFT energy level calculation pattern.

X-ray analysis

Fig. 4 shows the results of X-ray diffraction (XRD) measurements taken for analysis of polymer ordering structure. Fig. 4(a) shows the XRD results of polymer file measured in out-of-plane mode. PBDPBT-T and PBDPBT-biT films (100) had diffraction peaks appearing at 4.23, 4.41, 4.26 and 3.87°. Calculation by Bragg's law ($\lambda = 2d\sin\theta$) showed that highly ordered (100) lamellar d-spacing (d_1) was 20.72, 19.84, 20.74 and 22.85 Å. The crystal planes (010) associated with π–π stacking of the 4 polymers appeared respectively at 23.89, 24.94, 25.05 and 0°. The π–π stacking distance (d_π) calculated by Bragg's law was 4.14, 3.50 and 3.55 Å. In the case of PBDPOx-biT and PQcOx-TT (linear shaped polymer) with small d_π, formed more effective intermolecular π electron overwrap than the other two polymers. Moreover, PBDPOx-TT showed almost no peak, confirming that it had relatively very low crystallinity.

This indicated that the polymers formed (h00) lamellar structure and (0h0) lamellar structure together. Accordingly, when the π–π stacking peaks are observed on the (010) surface in out-of-plane mode, it is possible for the crystalline structure within the polymer film to form a face-on orientation, which can be confirmed by XRD measurement in in-plane mode. Fig. 4(b) shows the XRD results of polymer films in in-plane mode. PQcOx-biT show very small diffraction peaks at both low and high angles. However, the remaining 3 polymers showed relatively strong peaks. In particular, the polymers with linear shape, PBDPOx-biT and PQcOx-TT, showed relatively strong crystallinity. Through this, it was confirmed that polymers with linear shape have strong crystallinity and effective intermolecular π-electron overwrap. This was consistent with red-shift occurring from strengthening of intermolecular interactions when PBDPOx-biT and PQcOx-TT formed films, as seen in UV–vis absorption spectra.

Table 3
Optical and electrochemical properties of the polymers.

Polymer	UV–vis absorption				$E_g^{op,a}$ [eV]	Yield (%)	Cyclic voltammetry	
	$CHCl_3$ solution		Film				HOMO[b] [eV]	LUMO[a] [eV]
	λ_{max} [nm]	ε (10^4 M^{-1} cm^{-1})	λ_{max} [nm]	λ_{onset} [nm]				
PBDPOx-TT	413, 564	50,600	421, 563	708	1.75	72	−5.39	−3.64
PBDPOx-biT	441, 569	67,100	478, 591	733	1.69	88	−5.24	−3.55
PQcOx-TT	414, 556	57,300	416, 563	663	1.87	78	−5.30	−3.43
PQcOx-biT	401, 550	43,300	396, 547	700	1.77	85	−5.26	−3.49

[a] Calculated from the intersection of the tangent on the low energetic edge of the absorption spectrum with the baseline.
[b] $E_{HOMO\ (or\ LUMO)} = -[E_{onset}(vs\ Ag/AgCl) - E_{1/2}(Fc/Fc^+\ vs\ Ag/AgCl)] - 4.8$ eV.

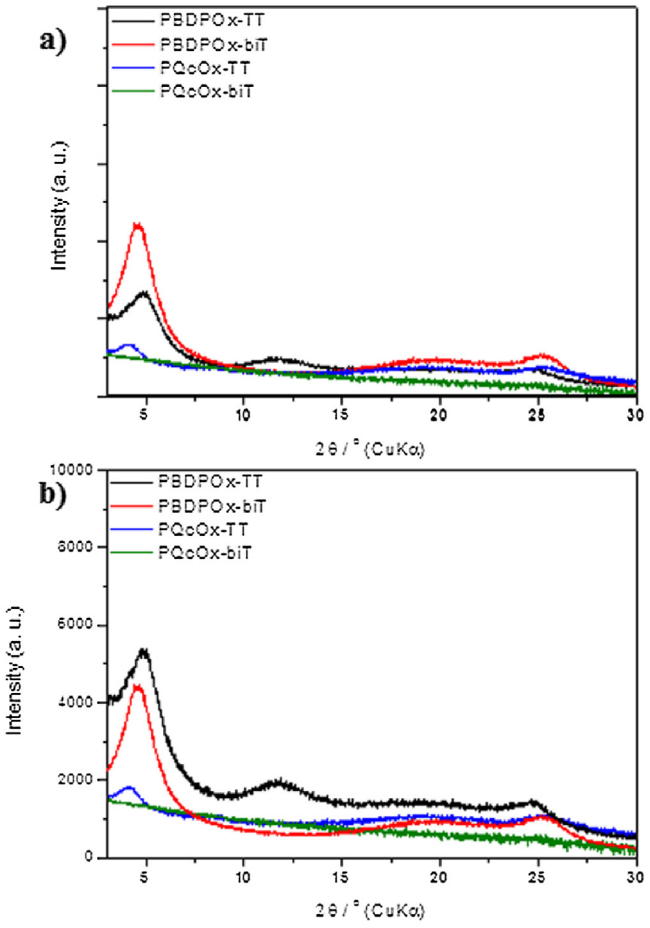

Fig. 4. X-ray diffraction patterns of the copolymer films on (a) out-of-plane mode and (b) in-plane.

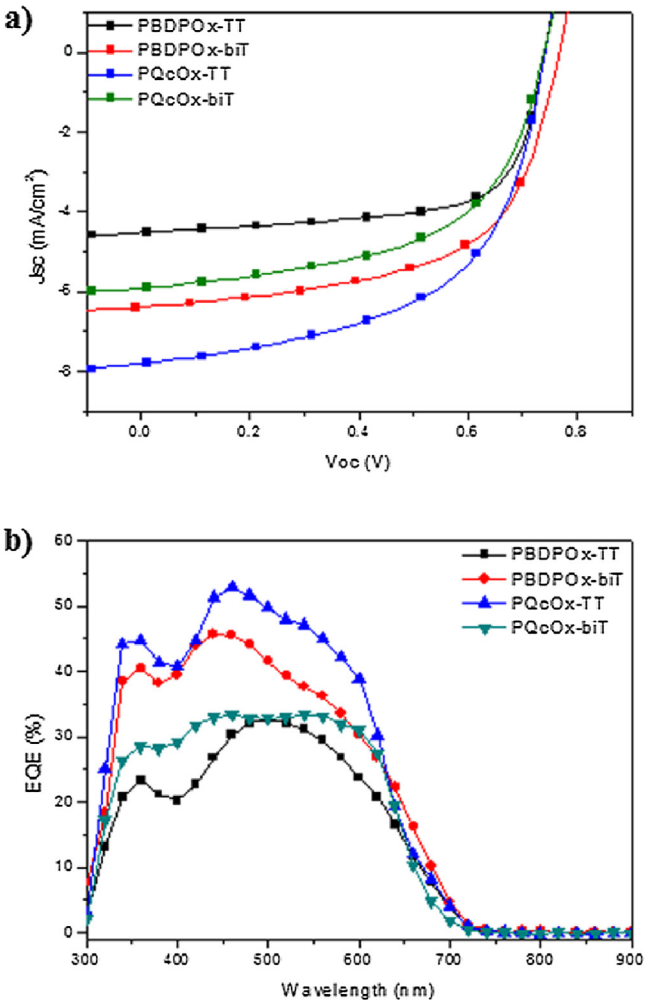

Fig. 5. (a) J–V characteristics and (b) external quantum efficiency of photovoltaic devices.

Photovoltaic properties

Conventional BHJ PSCs were fabricated for examining the photovoltaic (PV) properties of the synthesized polymers. In Fig. 5(a) shows the J–V curves of polymer: $PC_{70}BM$ (1:2 w/w%) blend photovoltaic device and (b) shows the IPCE spectra of these devices. The measure results are summarized in Table 4.

PBDPOx-biT and PQcOx-TT showed relatively higher PCE than PBDPOx-TT and PQcOx-biT which used the same donor acceptor chromophore. Voc of fabricated devices, polymers showed similar pattern as HOMO level measured in CV and DFT. Moreover, it was also confirmed that similar values were obtained because they used the same chromophore. However, PBDPOx-biT and PQcOx-TT had linear and planar structure, exhibiting a face-on riched structure, and as a result, showed improvement in J_{SC} of 20.8% and 39.7% as compared to PBDPOx-TT and PQcOx-biT, respectively.

For accuracy of J_{SC} measurements, external quantum efficiency (EQE) was measured. These devices showed sufficiently wide EQE graphs in the visible range (300–700 nm). Although large EQE values were seen in the absorption range of 300–700 nm, the EQE values decreased at ≥600 nm. PBDPOx-TT and PBDPBT-biT with linear main chain shape showed EQE_{max} value of 45.3 and 54.1%, respectively, but PBDPOx-TT and PQcOx-biT showed EQE_{max} of 32.4 and 33.1%. This was due to decreased exciton recombination caused by blending and PCBM according to steric hindrance and shape curvature [11,42]. J_{SC} could be calculated by using the integrated values from EQE graphs and those values were found to be similar to the values measured via an IV curve.

Morphology

Surface morphology of a polymer blend is a critical factor that determines the efficiency of PSCs. Therefore, atomic force microscopy (AFM) of film was measured from polymer:$PC_{70}BM$ (1:2 w/w%) blend with same conditions as the devices, the results of which are shown in Fig. 6. PBDPOx-biT:$PC_{70}BM$ and PQcOx-TT:$PC_{70}BM$ blend film showed small root-mean-square (RMS) roughness of 0.53 and 0.48 nm, respectively. They showed nanascale features in comparison to PBDPOx-TT:$PC_{70}BM$ blend film (4.41 nm RMS roughness) and PQcOx-biT:$PC_{70}BM$ blend film (6.20 nm RMS roughness). A small nano-network channel of polymer and PCBM had formed, while smooth morphology was shown. Rough morphology decreases charge separation on the active layer and it also increases exciton diffusion length, resulting in low photocurrent from increased charge recombination [43,44]. The results were the same as the shape curvature and steric hindrance values derived through DFT calculation. This was highly consistent with PBDPOx-TT and PQcOx-biT showing lower photocurrent than PBDPOx-biT and PQcOx-TT. The Mn of the PQcOx-biT (32,800 g/mol) was greater than that of PQcOx-TT (19,300 g/mol). The migration of charge carriers was facilitated by the formation of a charge transport pathway in the ordered region by making contact with the long polymer backbones [45]. The enhanced phase separation may be beneficial for charge extraction

Table 4
Photovoltaic devices performances of the polymers.

Polymer	$PC_{70}BM$ ratios	J_{SC} [mA/cm^2]	Calc. J_{SC} [mA/cm^2]	Voc [V]	FF [%]	EQE [%]	PCE [%]
PBDPOx-TT	1:2	5.3	4.84	0.75	58.7	32.4	2.4
PBDPOx-biT	1:2	6.4	6.31	0.78	59.8	45.3	3.3
PQcOx-TT	1:2	8.1	7.46	0.76	51.9	54.1	3.4
PQcOx-biT	1:2	5.8	5.24	0.74	54.8	33.1	2.4

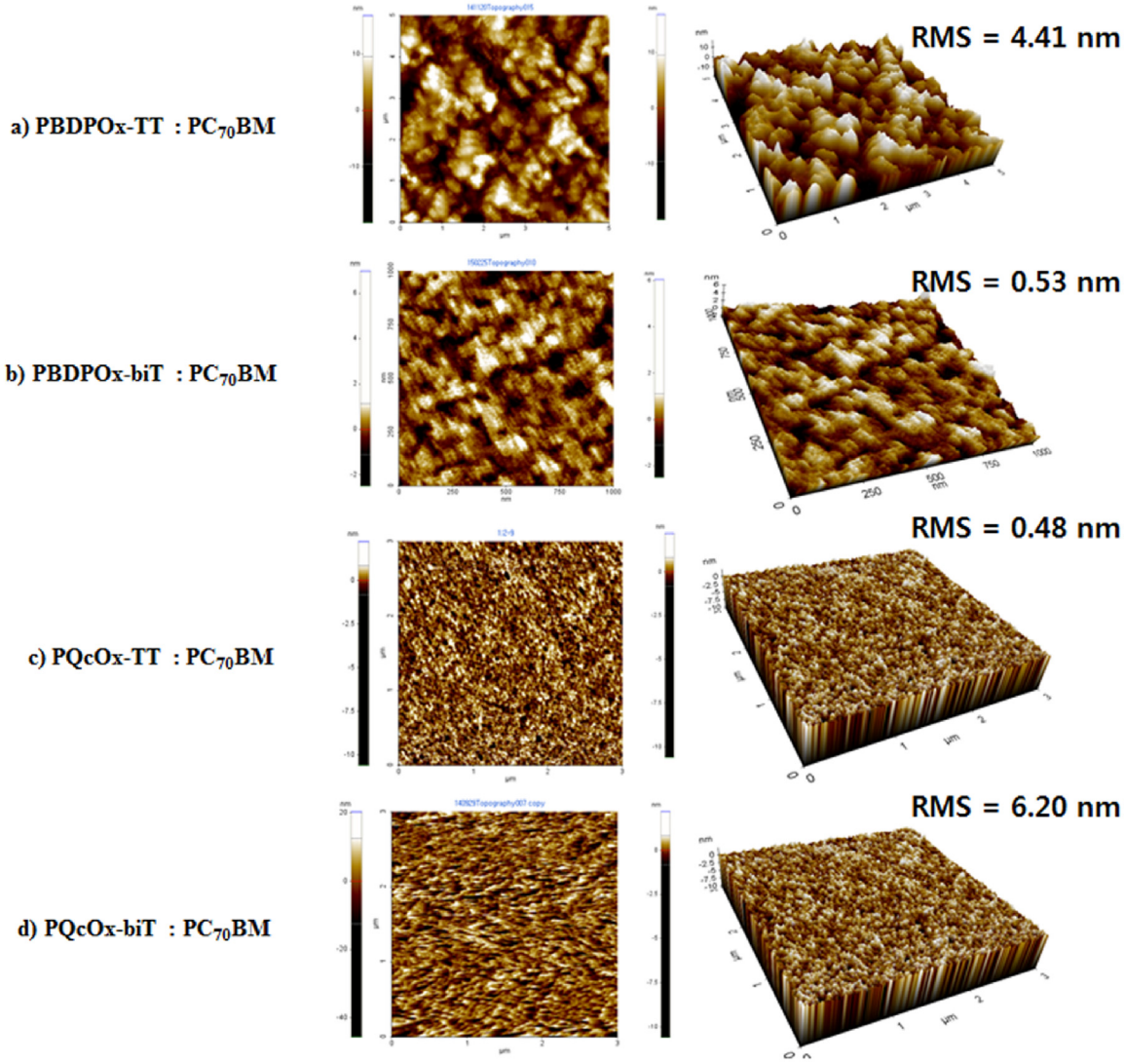

Fig. 6. Topographic AFM images of polymer:$PC_{70}BM$ blend films.

and for effectively suppressing the bimolecular recombination and achieving a higher FF [46].

Conclusion

We used Stille and Suzuki cross coupling in polymerizing PBDPOx-TT, PBDPBT-biT, PQcOx-TT and PQcOx-biT, D–A type polymers with BDP and Qc derivatives and Ox electron withdrawing unit as the electron donating unit, according to types of donor, acceptor and spacer monomer.

Polymers with 0 and 2 curved monomers formed planar and linear conformation in the direction of the main chain. It was also confirmed through UV–vis absorption and XRD meausrement results that they had face-on orientation and strong red-shifting of ≥10 mm on pristine polymer film from strong crystallinity. However, when only 1 was introduced, the monomer's curvature was not offset and curved conformation occurred from increase in the curved angle of the polymer main chain. As a result, on UV–vis spectroscopy, blue shift occurred on film, as compared to in solution. XRD measurements showed low crystallinity and only edge-on orientation.

In DFT, polymers with linear shape showed dihedral angle of close to 10°, showing values that have overall planar characteristics. Moreover, with respect to the shape of the main chain

backbone in DFT with 2 repeating units, PBDPOx-TT and PQcOx-biT had curved shape, making it difficult for even molecular alignment to be achieved. As a result, UV–vis absorption that was blue-shifted on film as compared to in solution was found, while low crystallinity and large π–π stacking distance were identified through XRD results.

This indicated that during the polymer design process, π-conjugation length can be increased according to donor and accepter monomer and π-spacer curved shape, and in addition, the shape of the polymer main backbone can be determined according to the curved shape of the monomer. This played an important role in intermolecular π-electron overwrap to impact the crystallinity of the polymer.

Therefore, PBDPOx-biT and PQcOx-TT, linear shaped polymers, showed higher PCE with higher J_{SC} values than PBDPOx-TT and PQcOx-biT, curve shaped polymers, while the best performance of PCE = 3.3% was found with PBDPOx-biT:$PC_{70}BM$ (1:2, w/w).

Acknowledgments

This research was supported by the New & Renewable Energy Core Technology Program of the Korea Institute of Energy Technology Evaluation and Planning (KETEP) grant funded by the Ministry of Trade, Industry & Energy (MI, Korea) (no. 20153010140030).

This work was supported by "Human Resources Program in Energy Technology" of the Korea Institute of Energy Technology Evaluation and Planning (KETEP), granted financial resource from the Ministry of Trade, Industry & Energy, Republic of Korea. (No. 20174010201540)

Appendix A. Supplementary data

Supplementary data associated with this article can be found, in the online version, at https://doi.org/10.1016/j.jiec.2018.04.029.

References

[1] A. Liang, G. Huang, S. Dong, X. Zheng, J. Zhu, Z. Wang, W. Wu, J. Zhang, F. Huang, J. Mater. Chem. C 4 (2016) 6626.
[2] I.R. de Moraes, S. Scholz, K. Leo, Org. Electron. 38 (2016) 164.
[3] Z. Yi, L. Ma, P. Li, L. Xu, X. Zhan, J. Qin, X. Chen, Y. Liu, S. Wang, Polym. Chem. 6 (2015) 5369.
[4] C. Constantinescu, A.K. Diallo, A. D'Aleo, F. Fages, P. Rotaru, C. Videlot-Ackermann, P. Delaporte, A.-P. Alloncle, Synth. Met. 209 (2015) 29.
[5] W. Li, K.H. Hendriks, A. Furlan, M.M. Wienk, R.A. Janssen, J. Am. Chem. Soc. 137 (2015) 2231.
[6] E. Pourbasheer, S. Morsali, A. Banaei, S. Aghabalazadeh, M.R. Ganjali, P. Norouzi, J. Ind. Eng. Chem. (Seoul Repub. Korea 26 (2015) 370.
[7] Q. An, F. Zhang, J. Zhang, W. Tang, Z. Deng, B. Hu, Energy Environ. Sci. 9 (2016) 281.
[8] M. Zhang, F. Zhang, Q. An, Q. Sun, W. Wang, J. Zhang, W. Tang, Nano Energy 22 (2016) 241.
[9] M. Zhang, F. Zhang, Q. An, Q. Sun, W. Wang, X. Ma, J. Zhang, W. Tang, J. Mater. Chem. A 5 (2017) 3589.
[10] X. Ma, Y. Mi, F. Zhang, Q. An, M. Zhang, Z. Hu, X. Liu, J. Zhang, W. Tang, Adv. Energy Mater. (2016) 1702854.
[11] L. Yang, L. Yan, W. You, J. Phys. Chem. Lett. 4 (2013) 1802.
[12] L. Ye, S. Zhang, L. Huo, M. Zhang, J. Hou, Acc. Chem. Res. 47 (2014) 1595.
[13] M. Löbert, A. Mishra, C. Uhrich, M. Pfeiffer, P. Bäuerle, J. Mater Chem. C 2 (2014) 4879.
[14] X. Wang, Y. Sun, S. Chen, X. Guo, M. Zhang, X. Li, Y. Li, H. Wang, Macromolecules 45 (2012) 1208.
[15] F. Livi, N.K. Zawacka, D. Angmo, M. Jørgensen, F.C. Krebs, E. Bundgaard, Macromolecules 48 (2015) 3481.
[16] Y. Ma, Q. Zheng, Z. Yin, D. Cai, S.-C. Chen, C. Tang, Macromolecules 46 (2013) 4813.
[17] Nicolas Blouin, Alexandre Michaud, David Gendron, Salem Wakim, Emily Blair, Rodica Neagu-Plesu, Michel Bellete^ te, Gilles Durocher, Ye Tao, Mario Leclerc, J. Am. Chem. Soc. 130 (2008) 732.
[18] H.Y. Chen, J. Hou, A.E. Hayden, H. Yang, K.N. Houk, Y. Yang, Adv. Mater. 22 (2010) 371.
[19] M. Wang, X. Hu, P. Liu, W. Li, X. Gong, F. Huang, Y. Cao, J. Am. Chem. Soc. 133 (2011) 9638.
[20] Q. Tao, Y. Xia, X. Xu, S. Hedström, O. Bäcke, D.I. James, P. Persson, E. Olsson, O. Inganäs, L. Hou, W. Zhu, E. Wang, Macromolecules 48 (2015) 1009.
[21] Y. Li, C.-Y. Chang, Y. Chen, Y. Song, C.-Z. Li, H.-L. Yip, A.K.Y. Jen, C. Li, J. Mater. Chem. C 1 (2013) 7526.
[22] T.H. Lee, M.H. Choi, S.J. Jeon, D.K. Moon, Polymer 99 (2016) 756.
[23] M.-H. Choi, H.Y. Kim, E.J. Lee, D. Kyung Moon, Polymer 91 (2016) 162.
[24] H.-J. Song, D.-H. Kim, E.-J. Lee, S.-W. Heo, J.-Y. Lee, D.-K. Moon, Macromolecules 45 (2012) 7815.
[25] T. Kashiki, M. Kohara, I. Osaka, E. Miyazaki, K. Takimiya, J. Org. Chem. 76 (2011) 4061.
[26] S. Göker, G. Hızalan, Y.A. Udum, L. Toppare, Synth. Met. 191 (2014) 19.
[27] Frank A. Arroyave, Coralie A. Richard, J.R. Reynolds, Org. Lett. 14 (2012) 6138.
[28] X. Wang, P. Jiang, Y. Chen, H. Luo, Z. Zhang, H. Wang, X. Li, G. Yu, Y. Li, Macromolecules 46 (2013) 4805.
[29] H. Yi, S. Al-Faifi, A. Iraqi, D.C. Watters, J. Kingsley, D.G. Lidzey, J. Mater. Chem. 21 (2011) 13649.
[30] W. Lee, G.-H. Kim, S.-J. Ko, S. Yum, S. Hwang, S. Cho, Y.-H. Shin, J.Y. Kim, H.Y. Woo, Macromolecules 47 (2014) 1604.
[31] I. Osaka, M. Saito, T. Koganezawa, K. Takimiya, Adv. Mater. 26 (2014) 331.
[32] C. Du, C. Li, W. Li, X. Chen, Z. Bo, C. Veit, Z. Ma, U. Wuerfel, H. Zhu, W. Hu, F. Zhang, Macromolecules 44 (2011) 7617.
[33] H.S. Lee, H.G. Song, H. Jung, M.H. Kim, C. Cho, J.-Y. Lee, S. Park, H.J. Son, H.-J. Yun, S.-K. Kwon, Y.-H. Kim, B. Kim, Macromolecules (2016), doi:http://dx.doi.org/10.1021/acs.macromol.6b01580.
[34] G. Zuo, Z. Li, M. Zhang, X. Guo, Y. Wu, S. Zhang, B. Peng, W. Wei, J. Hou, Polym. Chem. 5 (2014) 1976.
[35] J. Kim, N.H. Kim, S. Song, S.Y. Park, S. Chae, E. Bae, I. Kim, H.J. Kim, J.Y. Kim, H. Suh, Polymer 102 (2016) 84.
[36] P. Gautam, R. Misra, S. Biswas, G.D. Sharma, Phys. Chem. Chem. Phys. 18 (2016) 13918.
[37] M.-H. Choi, K.W. Song, D.K. Moon, Polym. Chem. 6 (2015) 2636.
[38] X. Guo, F.S. Kim, M.J. Seger, S.A. Jenekhe, M.D. Watson, Chem. Mater. 24 (2012) 1434.
[39] X. Zhang, A.J. Matzger, J. Org. Chem. 68 (2003) 9813.
[40] A. Prlj, B.F. Curchod, A. Fabrizio, L. Floryan, C. Corminboeuf, J. Phys. Chem. Lett. 6 (2015) 13.
[41] G. Brocks, A. Tol, J. Phys. Chem. 100 (1996) 1838.
[42] M. Wan, H. Zhu, J. Liu, L. Huo, RSC Adv. 5 (2015) 269.
[43] M. Chan Hwang, H. Kang, K. Yu, H.-J. Yun, S.-K. Kwon, K. Lee, Y.-H. Kim, Sol. Energy Mater. Sol. Cells 125 (2014) 39.
[44] T.E. Kang, H.-H. Cho, H.j. Kim, W. Lee, H. Kang, B.J. Kim, Macromolecules 46 (2013) 6806.
[45] D.H. Kim, H.J. Song, S.W. Heo, K.W. Song, D.K. Moon, Sol. Energy Mater Sol. Cells 120 (2014) 94.
[46] X. Li, H. Huang, H. Bin, Z. Peng, C. Zhu, L. Xue, Z.-G. Zhang, Z. Zhang, H. Ade, Y. Li, Chem. Mater. 29 (2017) 10130.